1-D Inversion of GREATEM Data by Supervised Descent Learning

Shan Lu, Bingyang Liang, Jianwen Wang, Feng Han, *Senior Member, IEEE*, and Qing Huo Liu, *Fellow, IEEE*

***Abstract*— In this letter, the application of the supervised descent method (SDM) for solving controlled-source electromagnetic inversion is studied. The descent direction in each iteration step of the 1-D full-wave inversion (FWI) is learned from the training data set with certain prior information in the off-line training and then saved. In the online prediction, it is directly combined with the measured data and the forward model to implement the FWI. Compared with the traditional iterative method, the efficiency is significantly enhanced since the computation of the Jacobian matrix is circumvented. Both the synthesized and field-measured grounded electrical-source airborne transient electromagnetic (GREATEM) data are used to verify the feasibility and efficiency of SDM. In addition, the learning ability of the SDM is also studied.**

***Index Terms*— Controlled-source electromagnetics (CSEM), full-wave inversion (FWI), supervised descent learning.**

I. Introduction

ELECTROMAGNETIC (EM) methods play an important role in the exploration of underground natural resources, such as water, ores, oil, and gas. The magnetotelluric (MT) and audio-magnetotelluric (AMT) methods utilizing passive sources, such as radio atmospherics, can provide underground conductivity information on the local and regional scales [1]. However, the effective EM signals are unstable and easily interfered with by noise. Meanwhile, the vertical resolution also decreases quickly as the exploration depth increases. The controlled-source electromagnetic (CSEM) is able to overcome these disadvantages [2] by using large-dimensional man-made coils or long cables. A typical CSEM system called the grounded electrical-source airborne transient electromagnetic (GREATEM) was proposed by Mogi *et al.* [3]. It uses a grounded electrical line source with a length of 2–3 km as the transmitter and a three-component magnetometer in the towing bird as the detector. The grounded horizontal line source transmits high-power EM waves that have a stronger penetration ability than the waves generated by the dipoles adopted in a traditional CSEM system [4].

Several deterministic inversion methods have been proposed to reconstruct the underground conductivity from CSEM data. They mainly include the Occam's method [5], Gauss–Newton [6], the Born iterative method (BIM) [7], distorted BIM (DBIM) [8], and so on. These methods can accommodate the large dimensions of the model parameters, which is crucial for 2-D or 3-D inversion problems. However, because these methods use the objective functions to quantify the mismatches of model parameters or measured data, time-consuming iterations are inevitable.

The artificial neural network (ANN) that completely discards the objective function and the iterations is another type of inversion method and has been successfully applied to the CSEM data [9]. The ANN is first trained by EM responses for typical conductive bodies or faults synthesized by the forward computation model and then used to efficiently predict the underground anomalies from the measured EM data. The supervised descent method (SDM) is another type of machine learning method that fuses the conventional iteration methods and the supervised learning technique. Specifically speaking, the machine learning module is embedded inside the iterations used to minimize the objective function and is to learn the Jacobian matrix [10]. This is different from the ANN in [9], which is completely treated as a black-box and must learn the complex underlying physics of EM scattering. Consequently, in the SDM, not only the physics of EM scattering remains in the objective function but also the online prediction becomes faster since the Jacobian matrix has been computed in the off-line training.

Previously, the SDM has been applied to the inversion of MT data [11] and logging-while-drilling data [12]. In this work, we perform the 1-D full-wave inversion of GREATEM data by using SDM. The system setups and data preprocessing of GREATEM have been discussed in [7] and [8]. This letter will focus on the implementation of SDM for GREATEM data and the comparison between SDM and the conventional DBIM. In Section II, the forward model, DBIM, and SDM are briefly introduced. In Sections III and IV, synthesized and field-measured data are respectively inverted by SDM to verify its feasibility and effectiveness. Finally, conclusions are drawn in Section V.

II. Method

A. Forward and Inversion Models

Fig. 1 shows the GREATEM survey of 1-D horizontal layered underground structure. The EM responses at the receiver coil excited by the $\hat{y}$-directional cable positioned in $y' = [-l \ \ l]$ and placed on the Earth surface can be

Manuscript received June 17, 2020; revised August 14, 2020, October 25, 2020, December 5, 2020, and January 16, 2021; accepted January 18, 2021. Date of publication February 1, 2021; date of current version January 4, 2022. This work was supported by the National Key Research and Development Program of the Ministry of Science and Technology of China under Grant 2018YFF01013300 and Grant 2018YFC0603503. *(Corresponding authors: Feng Han; Qing Huo Liu.)*

Shan Lu, Jianwen Wang, and Feng Han are with the Key Laboratory of Electromagnetic Wave Science and Detection Technology, Institute of Electromagnetics and Acoustics, Xiamen University, Xiamen 361005, China (e-mail: feng.han@xmu.edu.cn).

Bingyang Liang is with the College of Communication and Information Engineering, Xi'an University of Science and Technology, Xi'an 710054, China.

Qing Huo Liu is with the Department of Electrical and Computer Engineering, Duke University, Durham, NC 27708 USA (e-mail: qhliu@duke.edu).

Digital Object Identifier 10.1109/LGRS.2021.3053247

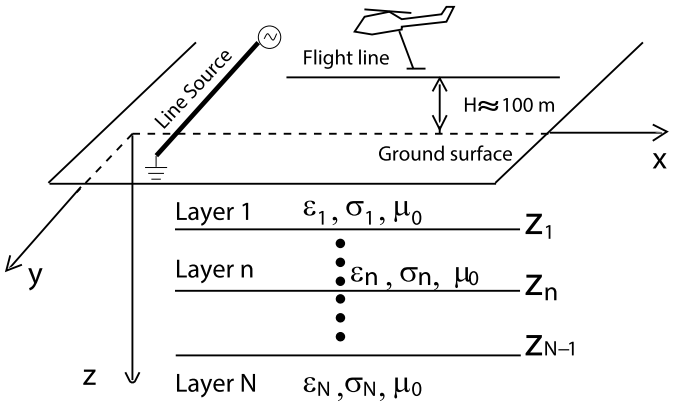

Fig. 1. Geometry for the GREATEM survey of the 1-D underground structure.

obtained by [8], [13]

$$H_x = \frac{1}{2\pi}\frac{y-l}{\rho_+}\int_0^\infty \left(I_i^e - I_i^h\right) J_1\left(k_\rho \rho_+\right) dk_\rho - \frac{1}{2\pi}\frac{y+l}{\rho_-}\int_0^\infty \left(I_i^e - I_i^h\right) J_1\left(k_\rho \rho_-\right) dk_\rho + \frac{1}{2\pi}\int_{-l}^{l}\int_0^\infty k_\rho I_i^h J_0\left(k_\rho \rho\right) dk_\rho dy' \tag{1a}$$

$$H_y = -\frac{1}{2\pi}\frac{x-x'}{\rho_+}\int_0^\infty \left(I_i^e - I_i^h\right) J_1\left(k_\rho \rho_+\right) dk_\rho + \frac{1}{2\pi}\frac{x-x'}{\rho_-}\int_0^\infty \left(I_i^e - I_i^h\right) J_1\left(k_\rho \rho_-\right) dk_\rho \tag{1b}$$

$$H_z = \frac{1}{2\pi}\frac{j}{\omega \tilde{\varepsilon}_v(z)}\int_{-l}^{l}\int_0^\infty \frac{x-x'}{\rho} k_\rho^2 V_i^h J_1\left(k_\rho \rho\right) dk_\rho dy' \tag{1c}$$

where k_ρ is the wavenumber in the $\hat{\rho}$ direction. I_i^p and V_i^p represent the equivalent current and voltage, and their definitions are given in [13]. J_0 and J_1 are the Bessel functions. ρ_+ and ρ_- are the horizontal distances from two ends of the line source to the receiver coil. The magnetic fields in (1) are actually computed by decomposing the spherical EM waves excited by the line source into a series of plane waves, evaluating the reflection and transmission coefficients for each component and, finally, implementing the integration in the spectral domain.

In the 1-D inversion, the model parameters of conductivities can be solved by DBIM. Details can be found in our previous work [8]. The DBIM is time-consuming since the Jacobian matrix (also called the Fréchet derivative matrix) must be updated in each iteration. Fortunately, this can be judiciously circumvented by SDM.

B. Supervised Descent Method

EM inversion is to seek the optimized model parameters by minimizing the data misfit between simulated data $\mathbf{F}(\mathbf{m})$ and measured data $\mathbf{d}^{\text{mea}}$

$$S(\mathbf{m}) = \|\mathbf{F}(\mathbf{m}) - \mathbf{d}^{\text{mea}}\|^2 \tag{2}$$

where $\mathbf{F}$ represents the forward modeling operator and $\|\|$ denotes the L_2-norm. $\mathbf{m}$ is the model parameter vector that contains the conductivities and layer positions. $\mathbf{d}^{\text{mea}}$ is the data vector that includes the measured magnetic fields at the receiver array. By applying the Taylor expansion to the misfit S at $\mathbf{m} = \mathbf{m}_0 + \Delta\mathbf{m}$ and minimizing it with respect to $\Delta\mathbf{m}$, we can easily obtain the perturbation quantity [10]

$$\Delta\mathbf{m} = \mathbf{K}(\mathbf{F}(\mathbf{m}_0) - \mathbf{d}^{\text{mea}}) \tag{3}$$

where $\mathbf{K} = -2\mathbf{H}_S^{-1}\mathbf{J}_F^T$ represents the descent direction. It is obvious that the computation of $\mathbf{K}$ is time-consuming since it contains the Hessian matrix $\mathbf{H}_S$ of the data misfit and the transpose of the Jacobian matrix $\mathbf{J}_F$. In SDM, $\mathbf{K}$ is trained offline by learning a linear regression between $\Delta\mathbf{m}$ and $\mathbf{F}(\mathbf{m}_0) - \mathbf{d}^{\text{mea}}$.

There are two strategies to reconstruct the model parameters from GREATEM data. One is the model-based for which both the layer boundary position and conductivity in each layer are reconstructed. The total layer number is usually fixed in the inversion although the layer boundary positions are allowed to change randomly. Another one is the pixel-based method. Each underground layer is divided into many thin layers. The conductivities in all the thin layers are reconstructed simultaneously. There is no requirement for the total layer number. The cost function in the kth iteration for SDM is constructed as [10]

$$\Phi_k^m = \|\left[\Delta\mathbf{C}_k^m, \Delta\mathbf{L}_k\right] - \Delta\mathbf{D}_k^m\mathbf{K}_k^{mT}\|_F^2 \tag{4}$$

for the model-based strategy, and

$$\Phi_k^p = \|\Delta\mathbf{C}_k^p - \Delta\mathbf{D}_k^p\mathbf{K}_k^{pT}\|_F^2 \tag{5}$$

for the pixel-based strategy. $\mathbf{C}^m$ and $\mathbf{C}^p$ denote the conductivity model parameter matrices used in the training for the model-based inversion and pixel-based inversion, respectively. The model parameter matrix $\mathbf{L}$ and the data matrix $\mathbf{D}$ include the layer boundary positions and measured data, respectively. These four matrices have the dimensions of $N \times M_m$, $N \times M_p$, $N \times L$, and $N \times R$, respectively. N is the number of the training set, M_m and M_p are the dimensions of unknown conductivity vectors in the model- and pixel-based inversion, respectively, L is the unknown layer position number, and R is the dimension of the measured data vector. The superscript T denotes the matrix transpose. The subscript F is the Frobenius norm, and Δ denotes the difference between true values and obtained values in the kth training step.

In the kth step of off-line training, the model parameters are input into the forward model to compute the field values at the receiver array. Then, the descent matrix $\mathbf{K}_k$ can be evaluated by minimizing (4) or (5). It is

$$\mathbf{K}_k^m = \left(\Delta\mathbf{D}_k^{mT}\Delta\mathbf{D}_k^m + \gamma\mathbf{I}\right)^{-1} \cdot \left(\Delta\mathbf{D}_k^{mT}\left[\Delta\mathbf{C}_k^m, \Delta\mathbf{L}_k\right]\right) \tag{6}$$

for the model-based inversion, and

$$\mathbf{K}_k^p = \left(\Delta\mathbf{D}_k^{pT}\Delta\mathbf{D}_k^p + \gamma\mathbf{I}\right)^{-1} \cdot \left(\Delta\mathbf{D}_k^{pT}\Delta\mathbf{C}_k^p\right) \tag{7}$$

for the pixel-based inversion. The parameter γ is the regularization factor used to facilitate the matrix inverse. It is determined by computing the mean value of all elements of $\Delta\mathbf{D}^T\Delta\mathbf{D}$ and dividing it with an empirical number, e.g., 100. The training will continue until the maximum number of iterations is reached, or the model and data misfits [10] are small enough. When the training terminates, the matrix $\mathbf{K}$ obtained in each step is saved. The flowchart of this learning process can be referred to [12].

TABLE I
MODEL PARAMETERS USED FOR TRAINING AND TESTING

	$\mathbf{m}_*$	$\mathbf{m}_1$	$\mathbf{m}_2$	$\mathbf{m}_3$	$\mathbf{m}_4$	$\mathbf{m}_0$
σ_1	4∼8	7.7	2	7.2	120	1
σ_2	10∼40	31	80	22	7.2	1
σ_3	100∼400	250	600	300	600	1
Z_2	100∼150	123	133	61	61	125
Z_3	300∼400	378	337	266	266	350

[1] The unit of σ is mS/m; the unit of Z is meter.
[2] $\mathbf{m}_*$ denotes the model parameters used in training; $\mathbf{m}_1$, $\mathbf{m}_2$, $\mathbf{m}_3$, and $\mathbf{m}_4$ are four sets of true model parameters for testing; $\mathbf{m}_0$ denotes the initial value.

In the kth step of online prediction, the unknown parameter is updated by

$$\mathbf{m}_{k+1} = \mathbf{m}_k + \mathbf{K}_k \Delta \mathbf{d}_k \tag{8a}$$

$$\Delta \mathbf{d}_k = \mathbf{d}^{\text{mea}} - \mathbf{d}_k \tag{8b}$$

where the model parameter vector $\mathbf{m}$ is the combination [see (4) and (5)] of conductivities and layer boundary positions in the model-based inversion and only the conductivity values of all the thin layers in the pixel-based inversion. In addition, one should note that the initial model $\mathbf{m}_0$ should be the same in the training and prediction.

III. NUMERICAL RESULTS

In this section, we apply the SDM to both model- and pixel-based inversions to validate its feasibility for GREATEM data. We also test the computational cost advantage of SDM over the conventional DBIM. Finally, the learning ability of SDM is studied. All the measured data are synthesized by the forward modeling algorithm. Both training and prediction are performed on a workstation with 48-core Xeon E5 2697 2.7G CPU, 512-GB RAM. The line source with the length of 2 km is placed in the $\hat{y}$-direction. The receiver array, including 201 receivers with the interval of 20 m, is orthogonal to the line source and placed 175 m above the ground. The frequencies used in the inversion are 20, 80, 160, and 300 Hz. Thus, the measured data vector has the dimension of 2412. In addition, in order to quantitatively evaluate the inversion error, we define the model misfits for conductivity and layer boundary positions as

$$\text{err}_\sigma = \frac{\| \log(\mathbf{m}_\sigma^{\text{inv}}) - \log(\mathbf{m}_\sigma^{\text{true}}) \|}{\| \log(\mathbf{m}_\sigma^{\text{true}}) \|} \tag{9a}$$

$$\text{err}_\text{L} = \frac{\|\mathbf{m}_L^{\text{inv}} - \mathbf{m}_L^{\text{true}}\|}{\|\mathbf{m}_L^{\text{true}}\|} \tag{9b}$$

where $\mathbf{m}_\sigma^{\text{inv}}$ is the inverted model vector containing the conductivity values in all layers, while $\mathbf{m}_\text{L}^{\text{inv}}$ is the inverted model vector containing the layer positions.

A. Applying SDM to GREATEM Data

It is assumed that there are three underground layers, and 100 random models are used to train the descent matrix $\mathbf{K}$. The ranges of the model parameters in the training are listed in Table I where σ_1, σ_2, and σ_3 are conductivities from the first layer to the third layer, and Z_2 and Z_3 are the lower boundaries of the first and second underground layers, respectively. In the pixel-based inversion, three underground layers are divided into 45 thin layers, and the lower boundaries of the first and second underground layers also randomly change in the ranges listed in Table I.

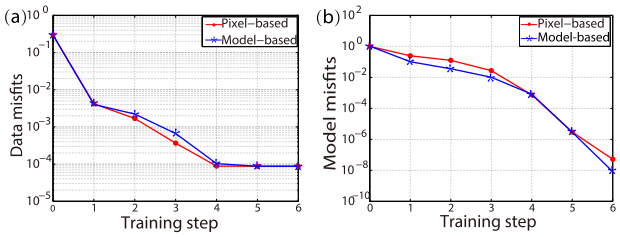

Fig. 2. Variations of (a) data misfits and (b) model misfits in the off-line training for two different inversion methods.

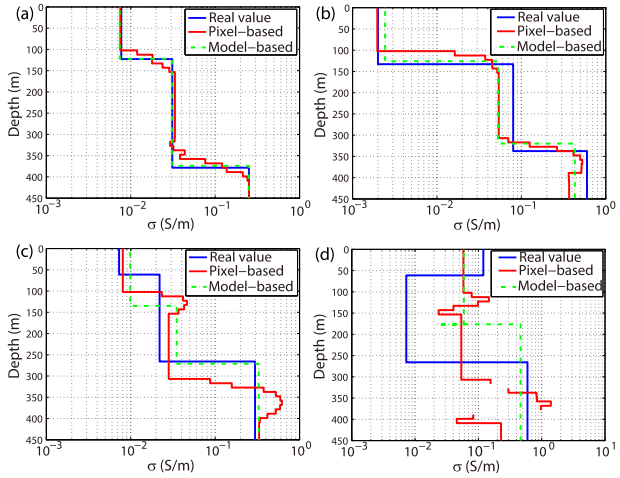

Fig. 3. Online prediction results for four models $\mathbf{m}_1$–$\mathbf{m}_4$ whose true model parameters are listed in Table I. (a) Both conductivities and layer positions within the training ranges. (b) Conductivities outside the training ranges but positions within the training ranges. (c) Conductivities within the training ranges but positions outside the training ranges. (d) Both conductivities and layer positions outside the training ranges.

As shown in Fig. 2, both model- and pixel-based training methods have fast convergence speeds, all converging within ten steps. However, the iteration speed is different. The model-based method takes 16 min in one step, while the pixel-based takes 37 min. The reason is that the sizes of matrices $\mathbf{K}$ in the two methods are different. It is 2412×7 in the model-based method but 2412×46 in the pixel-based method.

In the online prediction, we use the descent direction obtained in the off-line training to reconstruct the model parameters of the underground structure. The true model parameters for four tests are listed in Table I. As shown in Fig. 3(a), when the unknown layer positions and conductivities are both within the ranges of model parameters used in the training, both the model-based and pixel-based methods can reconstruct the underground structures well. However, the model-based method slightly outperforms the pixel-based for the reconstruction of sharp layer boundaries. When the conductivities are out the ranges of model parameters used in training, but the layer positions keep inside, the reconstruction error of conductivities is larger than that of layer positions, which is shown in Fig. 3(b). By contrast, as shown in Fig. 3(c), when the conductivities are inside the ranges, but the layer

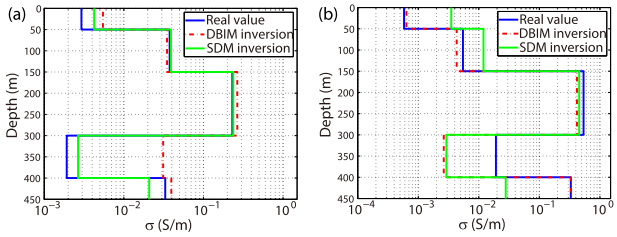

Fig. 4. Comparisons of inversion by SDM and DBIM. The synthetic measured data are contaminated by a 20-dB Gaussian white noise. (a) Conductivities within the training ranges. (b) Conductivities outside the training ranges.

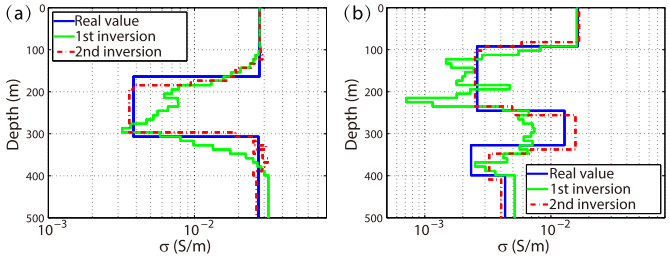

Fig. 5. (a) Three-layer model is included in the initial training data set. (b) Five-layer model is not included in the initial training data set.

positions are outside the ranges, the reconstruction error of conductivities is smaller than that of layer positions. However, it is noted that the conductivity and layer position have interaction for the SDM inversion. In other words, when one kind of model parameter exceeds the range in the training, the other one also cannot be well reconstructed. They couple with each other through the descent matrix **K**. When both the conductivities and layer positions are outside the training ranges, the reconstruction fails, as shown in Fig. 3(d).

B. Comparison With DBIM Inversion

We then compare the inversion by SDM and the conventional DBIM. We use the regularization strategy given in [14] for DBIM inversion. The measured data are synthesized by the forward solver with 20-dB Gaussian white noise added. Here, the noise level is defined according to the signal-to-noise ratio (SNR) of power. Since only the conductivity is reconstructed by DBIM in our previous work [8], we redesign the training model of SDM using the model-based inversion method in which there are five underground layers with their positions fixed. In the 200 training samples, the conductivity ranges between 1–50, 10–50, 100–500, 1–5, and 10–50 mS/m from the first to the fifth layer. As shown in Fig. 4, when the true conductivity values in all layers fall within the ranges of model parameters used in the training, SDM outperforms DBIM for the more accurate reconstruction in the deeper layers. The mean err_σ is 4.1% for the fourth and fifth layers in the SDM inversion but is 19.9% in the DBIM inversion. This obvious superiority of SDM for the reconstruction of deeper layers may be due to its strong adaptability to all kinds of noisy field data and underground layer configurations, which has been obtained in the training stage. However, when the true conductivities are outside the ranges, DBIM shows stronger adaptability. Another obvious difference is the computation time spent for the inversion. In each iteration step, SDM only needs 20 s, but the DBIM consumes around 30 min. This is because the descent matrix **K** has been computed in the off-line training of SDM and saved, but the Fréchet derivative matrix must be updated in each iteration of DBIM. One should note that the inversion time spent by SDM does not include the off-line training time.

C. Study of the Learning Ability

As discussed in Section III-B, SDM outperforms DBIM when proper prior information, e.g., the underground layer number and conductivity ranges, is incorporated into the training model. Unfortunately, these prior parameters are unavailable in many practical measurements. One solution is to diversify the training models. For example, in the beginning, we design 200 training samples and incorporate two-, three-, and four-layer models into them although the true underground structure only has three layers. The conductivity values range between 1 and 50 mS/m and the layer boundary positions change from 37 to 412 m in the training samples. The 1-D conductivity distribution obtained in the first inversion is shown in Fig. 5(a). Then, based on this preliminary result, we intuitively guess that the underground structure has three layers and, thus, redesign the training data set with only the three-layer model. After the off-line training is accomplished, the online prediction in the second inversion gives an underground structure close to the true model, as shown in Fig. 5(a). Then, we use the same training data set but change the real underground structure to five layers. The first inversion result in the SDM prediction is shown in Fig. 5(b). We can see that the five-layer structure still can be approximately reconstructed although it is not included in the training data set. Then, we redesign the training data set with only the five-layer model and perform the second inversion. The reconstructed underground structure is close to the true model, as shown in Fig. 5(b). The above analysis shows that SDM can still reconstruct the basic outline of the underground structure in the absence of prior information. It incorporates composite training models into its training data set and obtains the preliminary inversion result. Based on this, the training data set is updated to perform the prediction again to acquire a more accurate result. Therefore, SDM has a strong learning ability and adapts to multiple underground structures in the GREATEM measurements.

IV. Inversion of Field-Measured Data

In January 2016, the Changyi City in Shandong province of China was surveyed by a GREATEM system. The transmitter cable has a length of 2768 m, and a helicopter that moved in several flight lines with vertical heights of 115 m was used to collect the magnetic field data. The details of the measurements and the data preprocessing procedure were discussed in our previous work [8]. Here, we apply SDM to the measured data in the flight line C (see Fig. 11 of [8]) and compare the inversion result with that obtained by DBIM. We pick nine measurement points in flight line C, which are around 600–1700 m from the transmitter cable. The interval between the two measurement points is 120 m. In each point, ten frequencies, including 12, 19, 28, 41, 62, 91, 135, 200, 296, and 438 Hz, are used in the inversion. We apply the

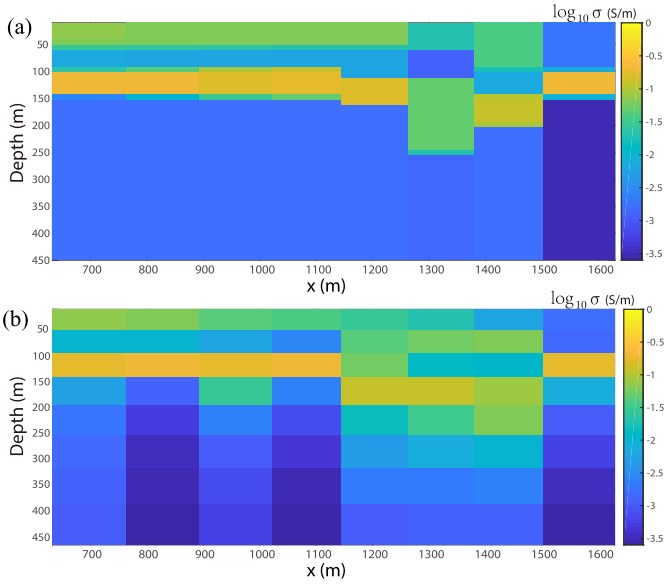

Fig. 6. Logarithm of conductivity obtained by inversion of field-measured data. (a) SDM inversion. (b) DBIM inversion.

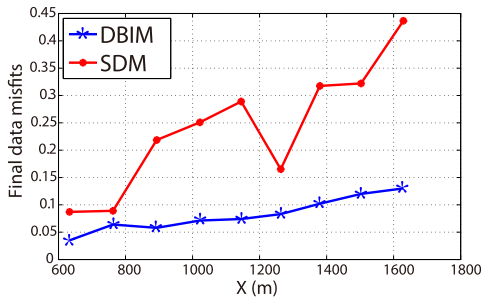

Fig. 7. Final data misfits of SDM and DBIM inversion when iterations end.

SDM and DBIM to the $\hat{z}$ component of the magnetic field data in each measurement point and integrate the 1-D profiles into a 2-D inversion diagram, as shown in Fig. 6. It should be noted that the pixel-based strategy is adopted, and the underground structure is divided into 45 thin layers. The conductivity values in the training vary from 0.1 to 0.4 S/m. The SDM results match the DBIM results well. It is shown that a high conductivity layer appears within 50 m below the Earth surface. In addition, at the depth of 100–150 m, another high conductivity band shows up. This is roughly consistent with the drilling data in this area. Just beneath the surface is the quaternary containing high conductivity material, which is followed by shale. Then, below the shale is a strip of iron ore that is followed by a thick granite layer.

Fig. 7 shows the final data misfits between computed and measured magnetic fields. Two observations are made: 1) the data misfits increase as the distance between the measurement point and the transmitter cable increases; this is because the SNR decreases as the distance increases and 2) SDM inversion has larger final data misfits than those of DBIM. Because no accurate prior information of the conductivity ranges of the underground structure is incorporated into the training data set of SDM, its adaptability to field-measured data is weaker than that of DBIM.

V. Conclusion

In this work, for the first time, SDM is applied to the inversion of semiairborne EM data. Compared with the conventional DBIM, SDM has the advantage of lower computational cost, supposing that proper prior information is incorporated into the training data set. It is due to the fact that the descent matrix in each iteration step of SDM has been computed and saved in the off-line training stage. However, when the prior information of the conductivity ranges of the underground structure is absent in the training, the adaptability of SDM is weaker than that of DBIM.

Numerical simulations show that SDM has a strong learning ability. When no prior information regarding the underground structure is available, SDM can still obtain reliable inversion results by incorporating composite training models and then refine them according to the preliminary prediction results. In addition, field-measured GREATEM data also verify the feasibility of SDM application to CSEM inversion.

References

[1] H. Cai and M. Zhdanov, "Three-dimensional inversion of magnetotelluric data for the sediment–basement interface," *IEEE Geosci. Remote Sens. Lett.*, vol. 13, no. 3, pp. 349–353, Mar. 2016.

[2] N. B. Boschetto and G. W. Hohmann, "Controlled-source audiofrequency magnetotelluric responses of three-dimensional bodies," *Geophysics*, vol. 56, no. 2, pp. 255–264, Feb. 1991.

[3] T. Mogi, Y. Tanaka, K. Kusunoki, T. Morikawa, and N. Jomori, "Development of grounded electrical source airborne transient EM (GREATEM)," *Explor. Geophys.*, vol. 29, nos. 1–2, pp. 61–64, Mar. 1998.

[4] X. Wang *et al.*, "Mapping deeply buried karst cavities using controlled-source audio magnetotellurics: A case history of a tunnel investigation in Southwest China," *Geophysics*, vol. 82, no. 1, pp. EN1–EN11, Jan. 2017.

[5] S. C. Constable, R. L. Parker, and C. G. Constable, "Occam's inversion: A practical algorithm for generating smooth models from electromagnetic sounding data," *Geophysics*, vol. 52, no. 3, pp. 289–300, Mar. 1987.

[6] M. Zaslavsky, V. Druskin, A. Abubakar, T. Habashy, and V. Simoncini, "Large-scale Gauss-Newton inversion of transient controlled-source electromagnetic measurement data using the model reduction framework," *Geophysics*, vol. 78, no. 4, pp. E161–E171, Jul. 2013.

[7] C. Qiu *et al.*, "Multifrequency 3-D inversion of GREATEM data by BCGS-FFT-BIM," *IEEE Trans. Geosci. Remote Sens.*, vol. 57, no. 4, pp. 2439–2448, Apr. 2019.

[8] B. Liang *et al.*, "A new inversion method based on distorted born iterative method for grounded electrical source airborne transient electromagnetics," *IEEE Trans. Geosci. Remote Sens.*, vol. 56, no. 2, pp. 877–887, Feb. 2018.

[9] V. Spichak, K. Fukuoka, T. Kobayashi, T. Mogi, I. Popova, and H. Shima, "ANN reconstruction of geoelectrical parameters of the minou fault zone by scalar CSAMT data," *J. Appl. Geophys.*, vol. 49, nos. 1–2, pp. 75–90, Jan. 2002.

[10] R. Guo, X. Song, M. Li, F. Yang, S. Xu, and A. Abubakar, "Supervised descent learning technique for 2-D microwave imaging," *IEEE Trans. Antennas Propag.*, vol. 67, no. 5, pp. 3550–3554, May 2019.

[11] R. Guo, M. Li, F. Yang, S. Xu, and A. Abubakar, "Regularized supervised descent method for 2-D magnetotelluric data inversion," in *Proc. SEG Tech. Program Expanded Abstr.*, Texas, TX, USA, Aug. 2019, pp. 2508–2512.

[12] Y. Hu *et al.*, "A supervised descent learning technique for solving directional electromagnetic logging-while-drilling inverse problems," *IEEE Trans. Geosci. Remote Sens.*, vol. 58, no. 11, pp. 8013–8025, Nov. 2020.

[13] K. A. Michalski and J. R. Mosig, "Multilayered media green's functions in integral equation formulations," *IEEE Trans. Antennas Propag.*, vol. 45, no. 3, pp. 508–519, Mar. 1997.

[14] Z. Yu, J. Zhou, Y. Fang, Y. Hu, and Q. H. Liu, "Through-casing hydraulic fracture evaluation by induction logging II: The inversion algorithm and experimental validations," *IEEE Trans. Geosci. Remote Sens.*, vol. 55, no. 2, pp. 1189–1198, Feb. 2017.